Simulating Space Weathering of a Carbonaceous Chondrite via Pulsed Laser Irradiation

Michelle Thompson[1], L. P. Keller[1], R. Christoffersen[2], M. J. Loeffler[3,4], R. V. Morris[1], T. G. Graff[2], and Z. Rahman[2]
[1]*ARES, NASA JSC, Houston, TX 77058*
[2]*Jacobs, NASA Johnson Space Center, Mail Code XI3, Houston, TX, 77058*
[3]*NASA GSFC, Greenbelt, MD 20771*
[4]*Northern Arizona University, Department of Physics and Astronomy, Flagstaff, AZ 86011*

Introduction: Grains on the surfaces of airless bodies are continually exposed to irradiation from solar wind ions and micrometeorite impact events. These processes, collectively known as space weathering, alter the microstructure, chemical composition, and spectral properties of surface soils [1-2]. While much work has been done to understand space weathering of lunar and ordinary-chondritic materials e.g., [3-5], the effects of these processes on hydrated carbonaceous chondrites is not yet well-understood. Analysis of the space weathering of carbonaceous materials will be critical for interpreting remote sensing reflectance data and for understanding the nature of samples returned by missions targeting primitive, organic-rich airless bodies, e.g., Hayabusa2 and OSIRIS-REx.

Prior to sample return, we can simulate space weathering processes in the laboratory. Micrometeorite impacts can be simulated through pulsed-laser irradiation, and recent experiments have shown the spectral properties of carbonaceous materials are altered by such simulated weathering events e.g., [6-8]. However, the resulting type of alteration i.e., reddening vs. bluing of the reflectance spectrum, is not consistent across all experiments. Further, the microstructural and crystal chemical effects of many of these experiments have not been well characterized, making it difficult to attribute spectral changes to specific mineralogical or chemical changes in the samples. Here we report results of pulsed laser irradiation experiments on chips of the Murchison CM2 carbonaceous chondrite to simulate micrometeorite impact processing.

Samples and Methods: We performed three separate pulsed laser experiments by scanning a Nd-YAG laser (wavelength of 1064 nm, average energy per pulse of 48 mJ, similar to [9]) (1) once, (2) twice, and (3) five times over the surface of the sample, in order to simulate various degrees of surface exposure. Glass slides were placed above the samples enabling the collection of the recondensed vapor plume produced by the irradiation, similar to [10]. We obtained reflectance spectra (0.3-2.5 μm) from unirradiated and 1x-irradiated samples, as well as of the vapor deposit of the 1x-irradiated sample. We have analyzed the morphological and chemical effects of the 1x-irradiated samples using the JEOL 7600F field emission scanning electron microscope (SEM) with x-ray detector system at JSC. From this sample, we have prepared electron transparent thin sections from the vapor deposit, the meteorite matrix, and several individual mineral phases using the FEI Quanta 3D focused ion beam (FIB) instrument. These sections were analyzed using the JEOL 2500SE scanning transmission electron microscope (STEM) equipped with a Thermo thin window energy-dispersive X-ray (EDX) spectrometer. We expect to make similar spectral measurements and prepare sections for STEM analysis for the 2x and 5x-irradiated sections.

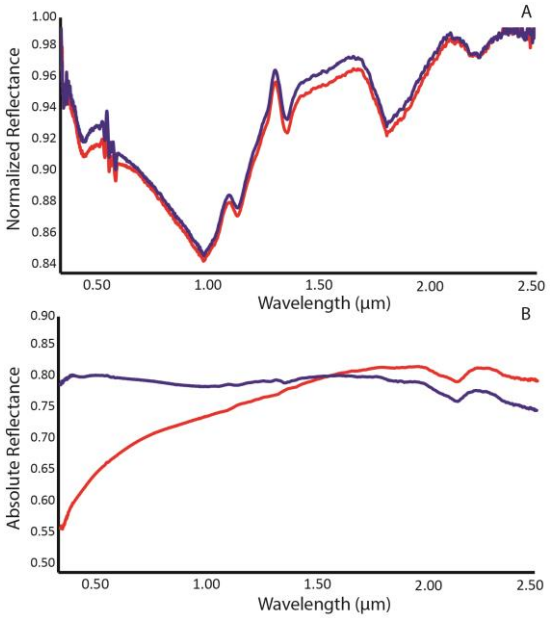

Figure 1: Reflectance spectra of the A) Surface of the irradiated Murchison meteorite (red) compared to the raw sample (blue), and B) The glass slide with the deposit on it (red) compared to the plain glass slide (blue).

Reflectance Measurements: The 1x-irradiated sample is darker (1-2%) than the unirradiated material (Fig. 1a) and the vapor deposit on the glass slide shows strong reddening through the VIS-NIR wavelengths (Fig. 1b).

Chemical and Structural Analysis: *Vapor Deposit:* The vapor deposit is microstructurally and chemically complex, composed of several individual layers ranging between 30-350 nm in thickness. The first layer is a uniform (~50 nm) amorphous layer containing embedded nanoparticles. Quantitative EDX maps indicate the composition of this layer is enriched in Fe, and includes S, Si, and O. Overlying this initial deposit in several locations are thicker (up to 250 nm) deposits composed of Mg, Si, Fe, and Ca (in localized regions). There are vesicles and nanoparticles distributed throughout this layer. The outermost layer is thin (30-50 nm) and EDX maps indicate it is enriched in volatile species including Fe and S, and includes embedded nanoparticles. The

nanoparticles distributed throughout the individual layers range in size from 2–30 nm in diameter and selected area electron diffraction (SAED) indicates at least three individual phases are present in the nanoparticle-bearing deposits including troilite (FeS), pentlandite ($(FeNi)_9S_8$), and magnetite (Fe_3O_4).

Matrix: The SEM images show the irradiated fine-grained matrix material has a distinctive 'frothy' texture, exhibiting sub-µm voids uniformly distributed across the surface. TEM analyses of the surface of the irradiated matrix provide evidence of melting including amorphous spherules and droplets. These melt products are up to 500 nm in thickness, are often vesiculated, and contain embedded nanoparticles. Quantitative EDX maps indicate the elemental composition of the melt layers includes Fe, Mg, Si, and S, although volatile species such as Fe and S are depleted in the melt layer relative to the underlying matrix. The matrix phases maintain crystallinity up to the boundary with the melt layer, with only localized regions of amorphization. The nanoparticles range in size from 5-50 nm and EDX maps indicate they are dominated by Fe-Ni-Sulfides.

Olivine: Bright-field STEM images of an olivine grain indicates there is an amorphous melt layer of uniform thickness (~15 nm) on the surface of the grain. EDX maps indicate this layer has an elemental composition that includes Ca, Al, Mg, Si, and Fe, with more refractory species like Ca and Al in higher concentrations than in the underlying grain. Superimposed on this refractory deposit is a thicker, irregular (up to 70 nm) amorphous layer with high concentrations of embedded nanoparticles ranging in size from 2-30 nm.

Fe-Ni-Sulfide: The surface of the Fe-Ni-Sulfide grain exhibits melt textures including droplet-like features. Dark-field STEM and correlated HRTEM images of the melted region indicate localized areas near the surface of have recrystallized. Vesicles are present within 500 nm of the surface and range in size from 5-100 nm. Quantitative EDX maps indicate there is no significant difference in the composition of the sulfide grain at the melted and recrystallized surface when compared to the interior region of the sample (Fig. 2).

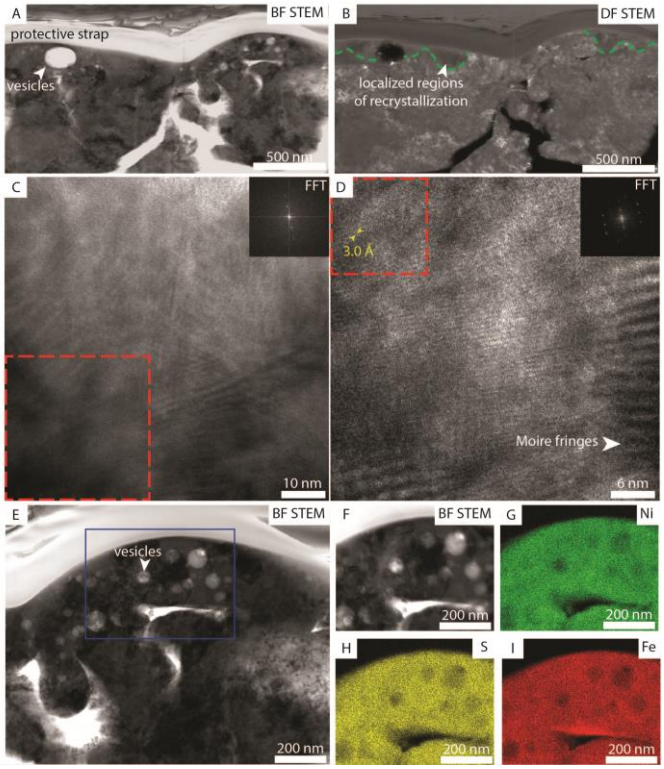

Figure 2: Analysis of the irradiated sulfide grain reveals A) melt features and vesicles in BF STEM, and B) areas of recrystallization in DF STEM, outlined by the dashed green lines. HRTEM images in C) and D) show zones of amorphization and short range order, highlighted by FFTs of regions bounded by the red dashed boxed. Measurements of the lattice fringes indicate spacings are consistent with pentlandite. Round vesicles are shown in E). The region outlined by the blue box in E) is shown in F). The chemical composition of this region is shown by EDX maps of G) Ni, H) S, and I) Fe, indicating the composition is consistent between the irradiated area and the underlying material.

Implications for Space Weathering of Primitive Bodies: The observed elemental fractionation between melt and vapor deposits influences the mineralogy of the nanoparticle population produced during space weathering events. The diversity of nanoparticle phases identified here indicates that the space weathering of carbonaceous materials is more complex than their lunar and ordinary chondrite-style counterparts. In addition, volatile species (including water) may play a significant role in the formation of space weathering features in carbonaceous surface materials. The prevalence of Fe-Ni-Sulfide and presence of Fe-Oxide nanoparticles may contribute to the unpredictable spectral behavior of some experimentally-produced samples. As such, an improved understanding of the optical characteristics of nanophase Fe-Ni-Sulfides is necessary to predict their effect on the spectral properties of airless body surfaces.

References: [1] Hapke B. 2001. Journal of Geophysical Research-Planets 106: 10,039-10,073. [2] Pieters C. M. and Noble S. K. 2016. Journal of Geophysical Research-Planets 121: 1865-1884. [3] Keller L. P. and McKay D. S. 1997. Geochimica et Cosmochimica Acta 61: 2331-2341. [4] Noguchi T. et al. 2014. Meteoritics and Planetary Science 49: 188-214. [5] Thompson M. S. et al. 2014. Earth, Planets, and Space 66: 1-10. [6] Sasaki S. et al. 2001. Nature 410: 555-557. [7] Loeffler M. J. et al. 2008. Icarus 196: 285-292. [8] Gillis-Davis J. J. et al. 2017. Icarus 286: 1-14. [9] Matsuoka M. et al. 2015. Icarus 254: 135-143. [10] Keller L. P. et al. 2013. Abstract 2404, 44th LPSC.